Chemical Science

ROYAL SOCIETY OF CHEMISTRY

EDGE ARTICLE

View Article Online
View Journal | View Issue

Cite this: *Chem. Sci.*, 2022, **13**, 10765

All publication charges for this article have been paid for by the Royal Society of Chemistry

Enantioselective synthesis of (−)-tetrabenazine *via* continuous crystallization-induced diastereomer transformation†

Andrew J. Kukor,[a] Noah Depner,[a] Isabelle Cai,[a] John L. Tucker,[b] Jeffrey C. Culhane[b] and Jason E. Hein *[a]

Received 30th March 2022
Accepted 23rd August 2022

DOI: 10.1039/d2sc01825j

rsc.li/chemical-science

A multi-well continuous CIDT approach with inline racemization of the solution phase is presented. Using two in-house built PATs and a flow reactor, we were able to successfully crystallize an enantiopure salt of TBZ, the active metabolite of the tardive dyskinesia drug valbenazine. Despite discovering an undesired racemic solid phase, inline racemization combined with careful control of crystallization conditions allowed for multigram quantities of enantiopure material to be harvested using our setup. Critically, this control was made possible by the use of PATs to observe and quantify the composition of both the solid and solution phases.

Introduction

Crystallization-induced diastereomer transformations

Crystallization can provide ready access to enantiopure materials,[1,2] and can be combined with solution-phase equilibria to drive chemical transformations.[3] In particular, crystallization-induced diastereomer transformations (CIDTs) have emerged in recent years as a means of obtaining enantiopure crystals from interconverting stereoisomers in solution.[4] CIDTs are typically performed as one-pot procedures which necessitate simultaneous stereoisomerization (*e.g.*, racemization) and crystallization. Significant screening and optimization are therefore required to develop a working CIDT process because racemization and crystallization require inherently different conditions. Rapid solution-phase chemical transformations frequently use acidic or basic additives and elevated temperatures. In contrast, additives can drastically alter crystallization behaviour and low temperatures maximize crystallization yields.[3] As such, a one-pot CIDT must compromise between the two processes, sacrificing the overall crystallization yield as a result.

Instead of using a one-pot procedure, rapid stereoisomerization and optimal crystallization conditions can both be achieved by continuously flowing solution between physically separate vessels dedicated to each process. This physical separation increases the yield of a CIDT process by limiting the amount of compound sequestered in elevated-temperature racemization solution. Such a two-well CIDT approach was recently demonstrated wherein solution was semi-continuously flowed between separate racemizer and crystallizer vessels,[5] producing the desired compound with >99% e.e. in up to 73% yield.[6] However, while physical separation may increase yields, dedicating an entire vessel to racemization risks exposing compounds to harsh conditions for prolonged periods, which could result in unwanted decomposition. Additionally, this two-well approach offers no control over crystallization beyond the temperature of the crystallization vessel and only works when there is no risk of undesired solid formation. Successful CIDTs require no decomposition and exclusive enantiopure solids formation, therefore making this two-well approach suboptimal in multicomponent systems where multiple solid phases are possible.

In lieu of a two-well setup, another hypothetical option could be a one-pot CIDT where the solution phase is continuously flowed through a heated external line to perform racemization. Such inline racemization would minimize the volume of solution held at elevated temperature, thereby maximizing yield and minimizing decomposition. However, this setup still offers limited control over crystallization beyond the chosen flow rate and crystallization temperature. Furthermore, one-pot CIDT procedures can only be operated in batches, which are subject to high degrees of variation and less efficient than continuous operation.[7] The reported two-well CIDT procedure[5,6] and this hypothetical one-well CIDT with inline racemization could both be operated in either a batch or semi-continuous manner, but still fail to meet the efficiency and control provided by continuous operation.

To afford careful control over crystallization conditions, we have designed a multi-well CIDT setup with physically separated

[a]*Department of Chemistry, The University of British Columbia, Vancouver, BC V6T 1Z1, Canada*

[b]*Neurocrine Biosciences, San Diego, California, 92130, USA*

† Electronic supplementary information (ESI) available. CCDC 2161840. For ESI and crystallographic data in CIF or other electronic format see https://doi.org/10.1039/d2sc01825j

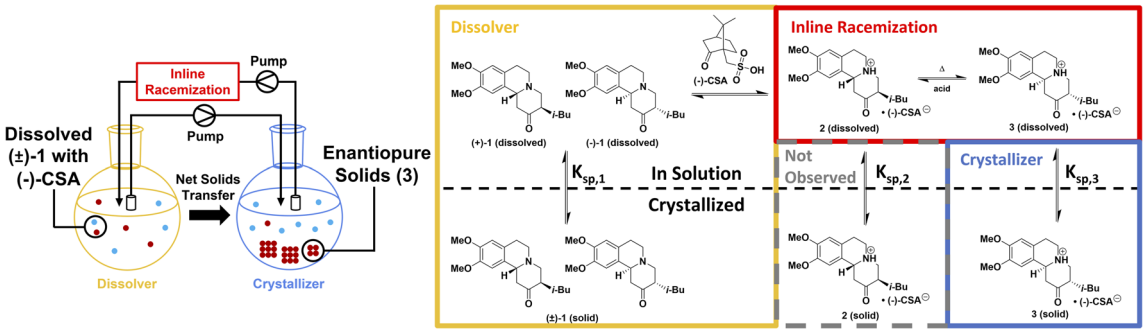

Fig. 1 Left: Conceptual diagram of continuous CIDT setup comprised of three physically separate regions: inline racemization (red), crystallization (blue), and dissolution (yellow). Solution phase is selectively transferred between flasks using pumps with inlet filters, with a temperature difference driving net transfer of solids to the crystallizer. Right: Illustration of processes occurring during tetrabenazine (TBZ) CIDT with (−)-camphorsulfonic acid ((−)-CSA): racemic TBZ solid ((±)-**1**) dissolution according to its solubility product (Ksp,1, left), solution-phase acid–base equilibrium with (−)-CSA (top left), solution-phase racemization of TBZ enantiomers (top right), and crystallization of TBZ·CSA salts **2** and **3** according to their respective solubility products Ksp,2 and Ksp,3 (with selective crystallization of **3** since Ksp,2 > Ksp,3).

dissolution and crystallization vessels, connected *via* inline racemization (Fig. 1, left). When operated continuously, this allows us to precisely control crystallization thanks to an additional dissolver flask. Firstly, selecting the temperatures of the dissolver and crystallizer flasks determines the solubilities (and therefore, the concentrations) in each vessel. Secondly, a physically separate dissolver flask allows racemic starting material to be added and enantiopure product to be harvested continuously, maximizing operating efficiency. Lastly, separating the crystallizer from the dissolver facilitates additional crystallization control *via* seeding, offering significant improvements over non-seeded approaches and ensuring undesired solids (such as racemic starting material) are never present in the crystallizer.

Unfortunately, despite the advantages afforded by continuous crystallization, careful control and optimization is required to produce a continuous process.[7] Additional measures must be taken when multiple solid phases are possible as one-pot CIDT procedures fail if undesired solids have similar solubilities to the desired enantiopure crystals.[3] For this reason, real-time data of continuous processes are invaluable, allowing for changes to be made on-the-fly and slight differences in solution and solids composition to be observed.

Monitoring crystallization with process analytical technology

A variety of process analytical technologies (PATs) are available to make such real-time measurements on continuously crystallizing systems, as outlined by a recent review.[8] Techniques such as online powder X-ray diffraction (PXRD),[9] focused beam reflectance measurement (FBRM),[10,11] particle vision and measurement (PVM)[12,13] and *in situ* Raman spectroscopy[14,15] allow for real-time solid phase characterization. Additionally, *in situ* Infrared (IR)[16,17] and Raman spectroscopy can provide solution-phase concentration data, with the latter also giving solid-phase composition information. However, such spectroscopic techniques suffer from dynamic range issues,[18] struggling to quantify impurities at the levels of interest to industrial applications.[19] This problem can be further exacerbated by temperature fluctuations interfering with *in situ* measurements,[20] as often occur during crystallizations. High performance liquid chromatography (HPLC) can be used with UV/vis spectroscopy to give a broader dynamic range for compositional analysis without suffering from *in situ* temperature effects, but is often performed in an offline fashion requiring manual sampling.[19]

While sampling from crystallizations can be challenging due to the presence of solids and supersaturation concerns, our lab has recently developed a tool that attaches to Mettler-Toledo's EasySampler probe. This modification allows for the selective sampling of the solution phase of crystallizations without clogging or probe fouling.[21] Combined with online HPLC analysis of samples,[22] we are able to obtain real-time solution phase component concentration data to track solution-phase equilibria, and even back-calculate the composition of the solid phase when the total system composition is known. Critically, this allows us to monitor solution-phase equilibria during a CIDT while simultaneously calculating solid phase yield and enantiomeric excess (e.e.) when chiral chromatography is used.[19]

Additionally, our lab has recently developed computer-vision based algorithms to analyze the turbidity of solutions.[23] Coupled to our CIDT, this allows us to track the presence and growth of solids in solution in real time using a webcam to feed images of the reactor to our algorithm. Two webcams can therefore be used to simultaneously track both the real-time dissolution of solids in the dissolver and their nucleation and growth in the crystallizer. Mettler-Toledo's EasyViewer probe can also be substituted for either webcam, allowing for microscopic imaging if desired.

We have therefore leveraged currently available PATs with custom-built tools to give us access to a variety of online measurements for both solid and solution phases. With these tools, we have developed a continuous, multi-well CIDT setup with inline racemization, applying it to a system with incompatible racemization and crystallization conditions. Using this system, we were able to control crystallization and obtain enantiopure crystals. This was despite the presence of a racemic

solid phase, which risked nucleating with (or instead of) the desired enantiopure solids if crystallization was not carefully controlled. This is a significant improvement to the literature-reported ability to access our desired molecule and serves as an example of how PAT tools can be used to similarly design other continuous crystallization processes.

Materials and methods

Solution-phase concentration data was obtained in the crystallizer using a custom-built thimble-shaped filter attachment to Mettler-Toledo's EasySampler probe.[21] This device makes use of the EasySampler's dynamic motion to perform *in situ* microfiltrations and avoid surface fouling while allowing the probe to selectively sample the solution phase. The sample is then delivered *via* tubing to an HPLC for online analysis using a setup similar to that previously demonstrated by our group.[22] By performing standard additions at the start of each experiment, this allowed us to convert the peak area measurements into concentrations for components of interest in the solution phase. Manual solid and solution phase samples were acquired for offline analysis to confirm these results.

Turbidity measurements were obtained *via* two methods. The first used a custom-built Python script developed by our lab to determine the turbidity of solutions based on the visual feed of a single webcam. A 3D-printed enclosure and LED lights were used to block exterior lighting and provide a constant source of illumination for these measurements, which could be used for both the crystallizer and dissolver flasks (see ESI† for details). Alternatively, Mettler-Toledo's EasyViewer probe was used when both turbidity and microscopic particle images were desired.

Inline racemization was studied using a Vapourtec R-series flow system comprised of two R2C+ modules and a R4 module with 10 mL internal reactor volume.

The multi-well CIDT setup with inline racemization used an EasyMax, IKA hotplate, and a custom-built 3D printed EasyMax well housing to allow inline racemization to occur. A 20 PSI backpressure regulator was used to facilitate racemization at temperatures above the solvent boiling point. Two Vapourtec SF-10 pumps were used to transfer solution between 100 mL EasyMax reactor vessels and the 7.4 mL inline racemization chamber.

Choice of analyte: tetrabenazine

We chose the CIDT of tetrabenazine (TBZ, **1**) to test our multi-well setup. TBZ is known to undergo a classical resolution process with (+)-camphorsulfonic acid ((+)-CSA) to form (+)-TBZ·(+)-CSA[24,25] providing access to (+)-TBZ, a precursor in the synthesis of the tardive dyskinesia drug valbenazine.[26,27] Additionally, TBZ is known to racemize with heat and acid or base (Fig. 1, right), and to additionally epimerize under these conditions to give undesired diastereomers. Our group has recently shown a Mannich-type reaction to be the final step in the synthesis of TBZ from ketone amine and isoquinoline derivatives,[28] supporting a racemization mechanism previously proposed for similar compounds (Fig. 2).[24] Notably, this mechanism is catalyzed by acid, and TBZ resolution is carried out using a chiral acid such as (+)-CSA. As such, enantiopure (+)-TBZ is obtained in >50% yields when the classical resolution with (+)-CSA is performed, indicating that a CIDT process is occurring.[25] However, TBZ racemization requires high temperatures which are unfavourable for crystallization, limiting the yields attainable from single batches. Iterative, labour-intensive crystallization–racemization batch cycles are therefore required for the CIDT of TBZ, and are the standard literature procedure for enantiopure (+)-TBZ·(+)-CSA isolation.[25,29] Furthermore, these high racemization temperatures risk TBZ decomposition, making this system a prime candidate for an alternative inline racemization approach.

Since our analytics were best able to resolve (−)-TBZ, we selected (−)-CSA as our chiral resolving agent and the (−)-TBZ·(−)-CSA diastereomeric salt (**3**) as our desired solid phase. Our powder X-ray diffraction spectrum of solid **3** exactly matched that reported for (+)-TBZ·(+)-CSA, indicating that our solid phase was its mirror image. The remaining (+)-TBZ in the system was assumed to crystallize as the (+)-TBZ·(−)-CSA salt **2** (Fig. 1, grey box) and have a higher solubility than **3**.

Results and discussion

Solvent selection

The solution phase of a multi-well CIDT is shared by all vessels (crystallizer, dissolver and racemizer), so selection of a solvent amenable to both racemization and crystallization was key. Given that the unit cell of (+)-TBZ·(+)-CSA is known to contain water[29] and the resolution of TBZ is reported in acetone,[25] we hypothesized that a mixture of acetone and water could facilitate racemization while controlling crystallization. As such, we screened the solubility of **3** in solvent mixtures of acetone and water. While this would normally be a long, labour-intensive process using standard protocols such as HPLC-based measurements, we were able to obtain solubility curves rapidly and autonomously for multiple solvent systems using our webcam turbidity tool (see ESI† for details). High solubility was desired for maximizing the rate of racemization, so the

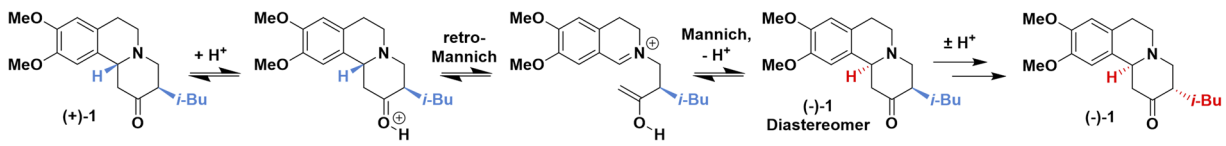

Fig. 2 Mechanism of (+)-TBZ ((**+**)-**1**) racemization into (−)-TBZ ((**−**)-**1**), illustrating interconversion in the presence of acid (*e.g.*, (−)-CSA) and heat.

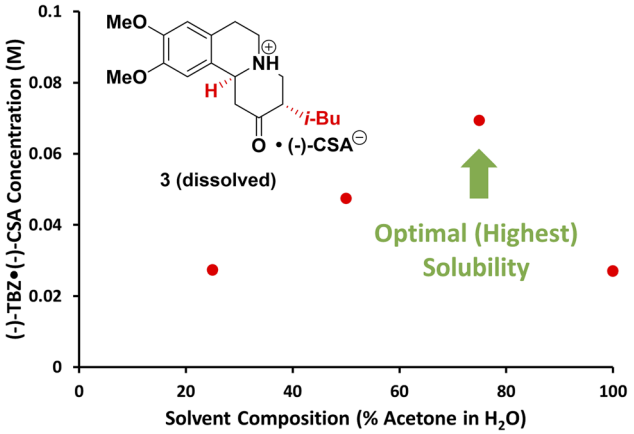

Fig. 3 Solubility of (−)-TBZ·(−)-CSA (**3**) at 25 °C in various solvent compositions, ranging from 100% acetone to 25% acetone/75% water (v/v), with conditions optimal for racemization and crystallization highlighted.

solvent mixture with the highest solubility of **3** was chosen: 75% acetone/25% water (Fig. 3).

Racemization optimization

Before investigating crystallization, racemization conditions needed to be established to find a solution phase compatible with both racemization and crystallization. Given that inline racemization was desired, a Vapourtec R-series flow system was used to investigate the effects of temperature and (−)-CSA equivalents on the rate of TBZ racemization. Despite (+)-TBZ racemizing into (−)-TBZ during the CIDT of TBZ with (−)-CSA, the availability of enantiopure **3** and the reversibility of the racemization mechanism (Fig. 2) prompted us to investigate the racemization of (−)-TBZ into (+)-TBZ (Fig. 4a).

Upon flowing (−)-TBZ solution with (−)-CSA through a heated coil, a clear link between temperature and racemization could immediately be seen with maximum racemization observed at 150 °C (Fig. 4b, blue). However, higher temperatures also gave rise to decomposition products (Fig. 4b, black). Since decomposition is extremely detrimental to a CIDT process,[4] it is necessary to use conditions highly selective for racemization over decomposition. This suggested that further optimization beyond temperature was necessary. When an additional 1.0 equiv. of (−)-CSA was added to the (−)-TBZ and (−)-CSA solution and passed through the flow system at 100 °C, racemization increased significantly and no decomposition of TBZ was observed (Fig. 4b, green). This confirmed the proposed acid-catalyzed racemization mechanism (Fig. 2) and prevented the need for additional reagents which may complicate crystal behaviour. As such, these conditions were selected for optimal racemization in our continuous CIDT process.

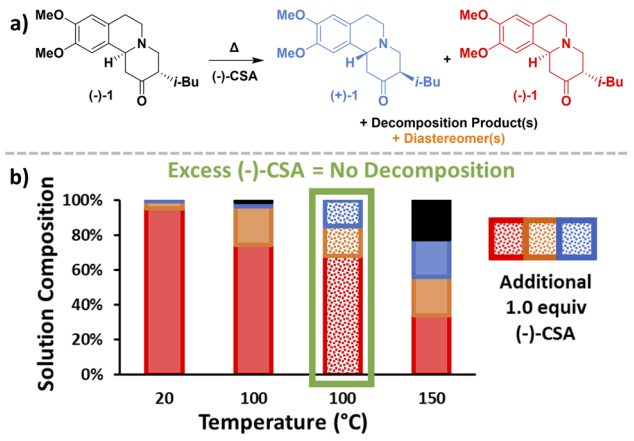

Fig. 4 Racemization of (−)-TBZ ((−)-**1**) in the presence of 1.0 equiv. (−)-CSA, dissolved in 75% acetone/25% water (0.01 M) using a Vapourtec flow system with a 10 minute residence time at 150 °C, and 0.025 M solution and 60 minute residence times for all other temperatures. Optimal conditions with no TBZ decomposition and significant racemization are highlighted in green.

Solid phase investigation

In addition to racemization, a successful CIDT process requires the desired solid phase to be both homochiral and the only polymorph formed under the reaction conditions.[4] Initially, we assumed that three solid phases were possible: racemic TBZ with no (−)-CSA ((±)-**1**), the desired (−)-TBZ·(−)-CSA solids (**3**), or undesired (+)-TBZ·(−)-CSA (**2**, grey box in Fig. 1). However, in a preliminary experiment we seeded the crystallizer flask with **3** and charged racemic starting material (±)-**1** to the dissolver, expecting exclusive crystal growth of enantiopure **3**. Instead, the crystallizer was found to contain only ∼70% e.e. of (−)-TBZ. Upon offline PXRD investigation, the sample was found to contain both **3** and a new racemic solid phase **4** (Fig. 5), indicating that careful control of crystallization is required to ensure that only enantiopure **3** forms during the CIDT process (see ESI† for details). Indeed, stepwise CIDT procedures in the literature limit the CSA used to 0.5 equiv. during the first resolution step,[25] avoiding formation of this undesired solid phase. However, further CSA addition provided ∼70% e.e. solid phases, suggesting growth of both **3** and **4** as we observed.

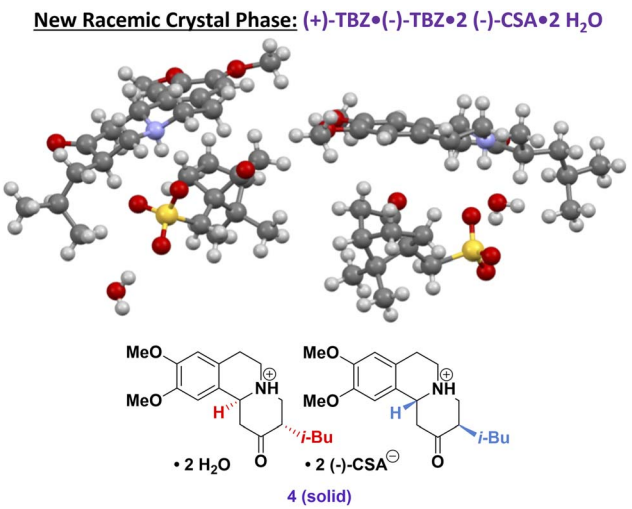

Fig. 5 Crystal structure of (−)-TBZ·(+)-TBZ·2(−)-CSA·2H_2O (**4**) illustrating the inclusion of both TBZ enantiomers in the unit cell. Additional crystallographic details may be found in the ESI.†

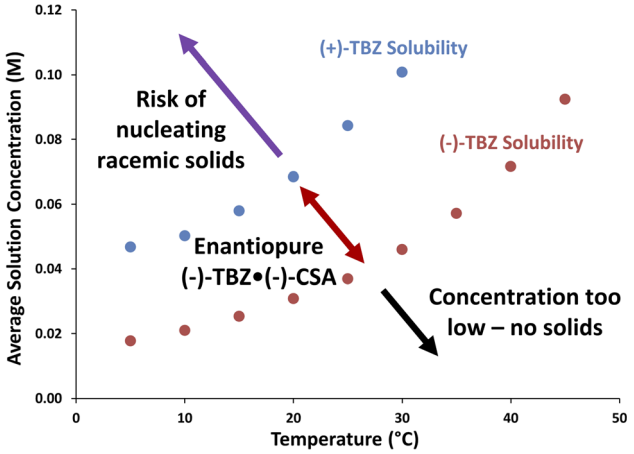

Fig. 6 Solubility curves for 25% water in acetone (v/v) containing racemic TBZ and 2.0 equiv. of (−)-CSA, with annotated phase behaviour indicating composition of solids obtained from each concentration/temperature regime. See ESI† for sample reproducibility and error analysis.

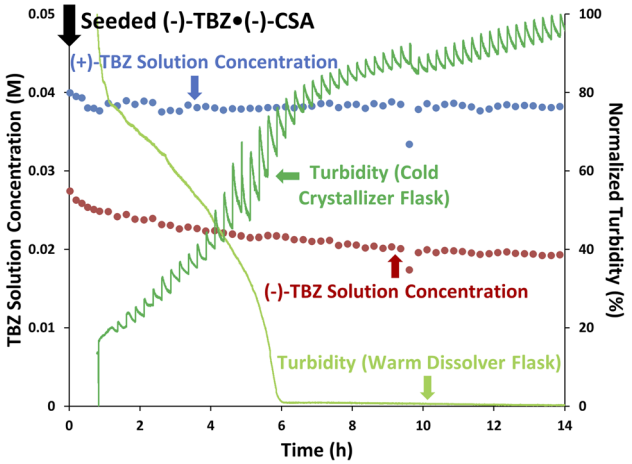

Fig. 7 Monitoring continuous crystallization of (−)-TBZ·(−)-CSA from a dissolver flask (24 °C) to a crystallizer flask (15 °C), demonstrating net solids transfer and controlled crystallization. TBZ solution concentrations were obtained with online HPLC and turbidity measurements with a webcam and custom-made computer-vision Python script.

Given the complex nature of the system, solubility curves for each TBZ enantiomer under the chosen conditions were desired to better understand crystallization behaviour. After adding racemic TBZ and 2.0 equiv. of (−)-CSA to 75% acetone/25% water, selectively sampling the solution phase while cycling the temperature resulted in solubility curves for each enantiomer (Fig. 6). Since the solid phase contained both TBZ enantiomers throughout this experiment, these solubility curves therefore represent the solution phase of a multicomponent solid-solution phase diagram. As such, Fig. 6 is not only a solubility diagram but also a phase diagram, indicating the composition of various solid phases that could be obtained by working above or below each solubility curve. It is evident from this data that high TBZ concentrations therefore risk crystallizing both TBZ enantiomers (Fig. 6, purple), and that careful control of CIDT operating conditions is necessary to obtain enantiopure solids.

CIDT testing: solids transfer

Having selected racemization and crystallization conditions, the three-well setup shown in Fig. 1 was assembled and tested (see ESI† for images of setup). Continuous crystallization of **3** was first performed with the dissolver at 24 °C and the crystallizer at 15 °C to demonstrate how real-time data can illustrate control over crystallization (Fig. 7). As solution was pumped between each vessel, a webcam was used to track the turbidity of each vessel using a custom-made computer-vision Python script. Since turbidity represents the amount of light being reflected by a mixture, the amount of solids present is therefore roughly correlated with the turbidity. As such, net solids transfer could clearly be seen from the increasing crystallizer turbidity (dark green) and concomitant decreasing dissolver turbidity (light green). Total solids dissolution was evident at 6 hours when the dissolver turbidity reached its minimum value, while continued solids evolution in the crystallizer could be seen as a slow increase in its turbidity after this point.

In addition to turbidity, online HPLC was used to monitor the solution-phase composition of the system by sampling from the crystallizer. Since a net solids transfer involves only dissolving solids from one flask (the dissolver) and crystallizing them out in another (the crystallizer), the solution phase composition should be constant throughout this process. As expected, there was little to no change in the (+)-TBZ solution concentration and only a slight decrease in the (−)-TBZ concentration. This confirmed that we were successfully controlling (−)-TBZ·(−)-CSA crystallization in the crystallizer flask despite the risk of nucleating racemic solids, as both trends would be expected to be decreasing if both enantiomers were crystallizing out. Manual sampling after 14 hours further validated this online HPLC data, as the crystallizer was found to contain >99% e.e. (−)-TBZ·(−)-CSA with virtually no (+)-TBZ in the solid phase.

CIDT testing: racemization

After ensuring we could control crystallization of **3** in the presence of (+)-TBZ, we added inline racemization to convert undesired (+)-TBZ into the desired enantiomer (Fig. 8). After (−)-TBZ·(−)-CSA seed crystals were added to crystallizer at 1 hour, the (−)-TBZ solution concentration could be seen to drop while (+)-TBZ stayed constant. Our online HPLC measurements therefore immediately confirmed that we successfully controlled crystallization by seeding and that none of racemic phase **4** was present, indicating we could continue with racemization of the enantioenriched solution phase composed primarily of (+)-TBZ.

As the CIDT continued and (+)-TBZ-enriched solution was flowed through the racemizer, the (+)-TBZ concentration decreased over time. This clearly indicated that the undesired (+)-TBZ was being racemized into (−)-TBZ. However, the turbidity in the crystallizer continued to increase throughout this process, suggesting that solids were forming in the crystallizer despite

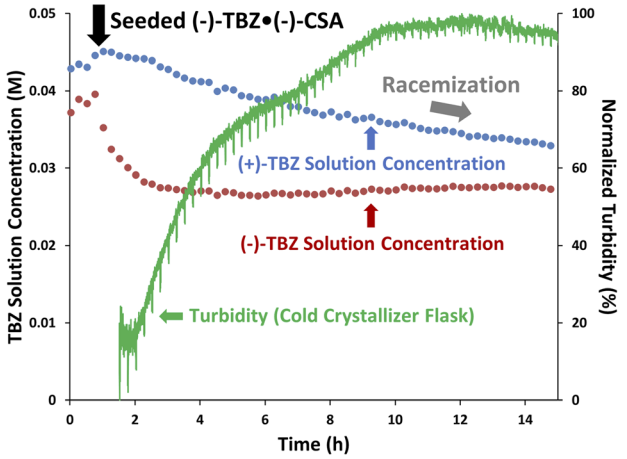

Fig. 8 Monitoring continuous CIDT of (−)-TBZ·(−)-CSA with added inline racemization, showing desired solid phase nucleation upon seeding and gradual racemization of (+)-TBZ into (−)-TBZ. The dissolver flask was held at 30 °C, the crystallizer flask at 15 °C and inline racemization performed at 100 °C.

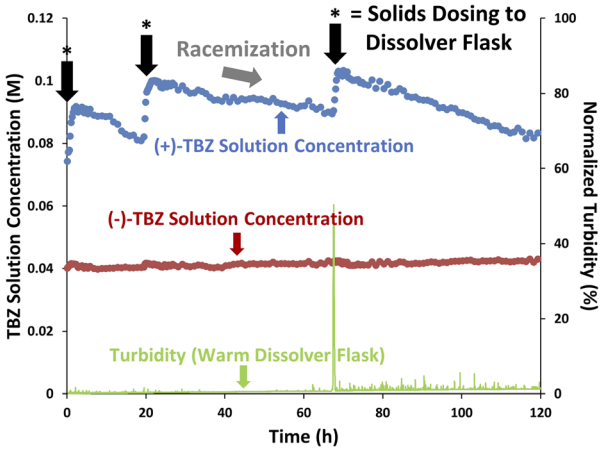

Fig. 9 Monitoring continuous CIDT of (−)-TBZ·(−)-CSA with solids dosing (* = 5.0 mmol of TBZ and (−)-CSA added) and inline racemization, illustrating how PAT informed dosing events. The dissolver flask was held at 33 °C, the crystallizer flask at 25 °C and inline racemization performed at 100 °C.

this (+)-TBZ depletion. If (+)-TBZ racemization were faster than (−)-TBZ·(−)-CSA solid nucleation, we might expect the (−)-TBZ solution phase concentration to increase over time. However, (−)-TBZ's concentration remained constant after seeding. This suggested that the newly-racemized (+)-TBZ was crystallizing out of the solution as soon as it was converted into (−)-TBZ *via* rapidly forming the less soluble (−)-TBZ·(−)-CSA salt (which was again >99% e.e. after the reaction). This in turn suggests two things: (1) the equilibrium between (−)-TBZ and (−)-CSA forming (−)-TBZ·(−)-CSA in solution is rapid, and (2) this solution phase equilibrium and the nucleation of solid (−)-TBZ·(−)-CSA are both faster than the racemization of (+)-TBZ.

In addition to letting us determine the relative rates of the solution phase acid–base equilibrium, racemization and nucleation, the quantitative nature of our online HPLC data allows us to determine the exact rate of racemization from the slope of the (+)-TBZ trend. As this rate was only 1.0 mM h^{-1}, this indicates that racemization is likely the limiting factor under these conditions. While higher concentrations should improve this rate, they also risk undesired solids nucleation if the temperature is not also increased (Fig. 6, purple). Higher operating temperatures were therefore desired for future experiments to increase the solubility of both TBZ enantiomers, and to therefore improve the rate of racemization while ensuring enantiopure (−)-TBZ·(−)-CSA was still selectively crystallized.

Final continuous CIDT demonstration

Given the above successful demonstrations of controlled crystallization and inline racemization, a continuous CIDT was attempted to produce enantiopure (−)-TBZ·(−)-CSA as racemic starting material was fed into the dissolver flask. The flasks were operated at higher temperatures than previously, with the dissolver now 33 °C *vs.* 30 °C and the crystallizer now 25 °C *vs.* 15 °C to increase the rate of racemization. Unfortunately, initial attempts produced racemic solids in the crystallizer flask after (+)-TBZ concentrations exceeded 0.1 M (see ESI† for details). Based on Fig. 6, it was proposed that at elevated temperatures the concentration of (+)-TBZ was too high for enantiopure (−)-TBZ·(−)-CSA to form. As such, smaller starting material solid doses to the dissolver flask were performed to maintain operation below (+)-TBZ's solubility and avoid nucleation of undesired solids (Fig. 9). The turbidity of this flask was monitored to ensure that undesired solids nucleation did not occur and that solid doses fully dissolved (light green trend).

Critically, informed solid dosing was made possible by the accurate, real-time concentration data provided by our online HPLC data. Since we previously encountered racemic solids when (+)-TBZ's concentration exceeded 0.1 M, (+)-TBZ solution concentration was monitored and starting material doses only performed when (+)-TBZ's concentration dropped to near 0.8 M. Each of these doses can clearly be seen in the (+)-TBZ solution phase trend as sudden spikes in concentration. These spikes once again show how our PATs can provide access to chemical and physical rate constants for our system (in this case, the rate of solution transfer).

As in the previous racemization experiment, the (+)-TBZ concentration dropped as racemization occurred and (+)-TBZ was converted into the desired (−)-TBZ. Again, no change in (−)-TBZ concentration was observed in the crystallizer flask during either racemization or dosing, suggesting that (−)-TBZ·(−)-CSA nucleation was faster than both racemization (which was clearly slow) and solution transfer (which was quite rapid).

Ultimately, after 2 weeks of continuous operation 18.39 g of enantiopure (−)-TBZ·(−)-CSA was harvested (>98% e.e., 48% yield). Neutralization and extraction of the solution phase indicated that at least 4.1 g of (−)-TBZ were additionally present in the system, giving a total system composition of 67% (−)-TBZ. This illustrates that although our process was slow, CIDT was clearly occurring and enantiopure solids could successfully be obtained on >10 g scale with continuous operation. Prolonged continuous operation could provide quantitative yields of

enantiopure (−)-TBZ·(−)-CSA if desired, and further optimization could be performed to improve the speed of this process if desired (especially by increasing the rate of racemization).

Conclusions

In summary, we have demonstrated the control over continuous crystallization afforded by physically separating the processes of racemization, dissolution and crystallization. We highlighted the utility of monitoring such processes with PATs to inform rational experimental design and real-time control of processes, using two novel PATs to track solid and solution phase behaviour of a continuous CIDT. With this data, we were able to selectively crystallize large quantities of enantiopure (−)-TBZ·(−)-CSA after monitoring the rates of various chemical and physical processes inherent to our system. We observed the rate of racemization to be the limiting factor for our process and avoided nucleating a newly discovered (undesired) racemic solid phase by informing dosing of starting material with our real-time PAT measurements.

Data availability

The ESI† contains experimental and hardware descriptions, product characterization data and analytical validation/calibration. Concentration *vs.* time data is included in .xls format. Novel crystal structures have been uploaded to CCDC.

Author contributions

AJK, JLT JCC and JEH conceptualized the project. AJK, ND and IC executed the experiments, performed the research and co-wrote the paper. JCC and JEH supervised the investigation. All authors analyzed the data, discussed the results and commented on the manuscript.

Conflicts of interest

There are no conflicts to declare.

Acknowledgements

The authors gratefully acknowledge Mettler-Toledo Autochem for their generous donation of process analytical equipment (EasyMax, EasySampler and EasyViewer) to JEH. Financial support for this work was provided by Neurocrine Biosciences Inc., The University of British Columbia, the Canada Foundation for Innovation (CFI) (CFI-35883) and the Natural Sciences and Engineering Research Council of Canada (NSERC) (RGPIN-2021-03168, Discovery Accelerator Supplement). Student support was provided by an NSERC CGS-D scholarship (AJK) and UBC's 4YF scholarship (ND). The authors also wish to thank Neurocrine Biosciences Inc. for donation of starting materials for compound synthesis, and AJK wishes to thank Tristan Maschmeyer for assistance with revision and data visualization.

References

1 G. Coquerel, *Top. Curr. Chem.*, 2006, **269**, 1–51.
2 M. Kaspereit, S. Swernath and A. Kienle, *Org. Process Res. Dev.*, 2012, **16**, 353–363.
3 A. Kolarovic and P. Jakubec, *Adv. Synth. Catal.*, 2021, **363**, 4110–4158.
4 K. M. J. Brands and A. J. Davies, *Chem. Rev.*, 2006, **106**, 2711–2733.
5 M. Guillot, J. de Meester, S. Huynen, L. Collard, K. Robeyns, O. Riant and T. Leyssens, *Angew. Chem., Int. Ed.*, 2020, **59**, 11303–11306.
6 M. Guillot, J. de Meester, L. Collard, O. Riant and T. Leyssens, *Org. Process Res. Dev.*, 2021, **25**, 884–891.
7 D. Zhang, S. Xu, S. Du, J. Wang and J. Gong, *Engineering*, 2017, **3**(3), 354–364.
8 J. Orehek, D. Teslić and B. Likozar, *Org. Process Res. Dev.*, 2021, **25**, 16–42.
9 R. B. Hammond, X. Lai, K. J. Roberts, A. Thomas and G. White, *Cryst. Growth Des.*, 2004, **4**(5), 943–948.
10 D. Acevedo, W.-L. Wu, X. Yang, N. Pavurala, A. Mohammad and T. F. O'Connor, *CrystEngComm*, 2021, **23**, 972–985.
11 I. I. Onyemelukwe, A. R. Parsons, H. P. Wheatcroft, A. Robertson, Z. K. Nagy and C. D. Reilly, *Cryst. Growth Des.*, 2019, **19**, 66–80.
12 G. Hou, G. Power, M. Barrett, B. Glennon, G. Morris and Y. Zhao, *Cryst. Growth Des.*, 2014, **14**, 1782–1793.
13 L. Dang, H. Yang, S. Black and H. Wei, *Org. Process Res. Dev.*, 2009, **13**(6), 1301–1306.
14 D. Acevedo, X. Yang, A. Mohammad, N. Pavurala, W.-L. Wu, T. F. O'Connor, Z. K. Nagy and C. N. Cruz, *Org. Process Res. Dev.*, 2018, **22**, 156–165.
15 K. A. Powell, A. N. Saleemi, C. D. Rielly and Z. K. Nagy, *Org. Process Res. Dev.*, 2016, **20**, 626–636.
16 H. Siddique, C. J. Brown, I. Houson and A. J. Florence, *Org. Process Res. Dev.*, 2015, **19**, 1871–1881.
17 V. Raval, H. Siddique, C. J. Brown and A. J. Florence, *CrystEngComm*, 2020, **22**, 2288–2296.
18 L. T. Hagemann, M. M. McCartney, A. G. Fung, D. J. Peirano, C. E. Davis and B. Mizaikoff, *Analyst*, 2018, **143**(23), 5683–5691.
19 A. Cote, D. Erdemir, K. P. Girard, D. A. Green, M. A. Lovette, E. Sirota and N. K. Nere, *Cryst. Growth Des.*, 2020, **20**, 7568–7581.
20 G. Févotte, *Chem. Eng. Res. Des.*, 2007, **85**(7), 906–920.
21 A. J. Kukor, M. A. Guy, J. M. Hawkins and J. E. Hein, *React. Chem. Eng.*, 2021, **6**, 2042–2049.
22 T. C. Malig, J. D. B. Koenig, H. Situ, N. K. Chehal, P. G. Hultin and J. E. Hein, *React. Chem. Eng.*, 2017, **2**(3), 309–314.
23 P. Shiri, V. Lai, T. Zepel, D. Griffin, J. Reifman, S. Clark, S. Grunert, L. P. E. Yunker, S. Steiner, H. Situ, P. L. Prieto and J. E. Hein, *iScience*, 2021, **24**, 3.
24 H. T. Openshaw and N. Whittaker, *J. Chem. Soc.*, 1963, 1461–1471.
25 Z. Yao, X. Wei, X. Wu, J. L. Katz, T. Kopajtic, N. H. Greig and H. Sun, *Eur. J. Med. Chem.*, 2011, **46**(5), 1841–1848.

26 D. E. Grigoriadis, E. Smith, S. R. J. Hoare, A. Madan and H. Bozigian, *J. Pharmacol. Exp. Ther.*, 2017, **361**, 454–461.
27 H. Skor, E. B. Smith, G. Loewen, C. F. O'Brien, D. E. Grigoriadis and H. Bozigian, *Drugs R&D*, 2017, **17**, 449–459.
28 Y. Sato, J. Liu, A. J. Kukor, J. C. Culhane, J. L. Tucker, D. J. Kucera, B. M. Cochran and J. E. Hein, *J. Org. Chem.*, 2021, **86**, 14069–14078.
29 Q. Yu, W. Luo, J. Deschamps, H. W. Holloway, T. Kopajtic, J. L. Katz, A. Brossi and N. H. Grieg, *ACS Med. Chem. Lett.*, 2010, **1**, 105–109.